THE JOURNAL OF PHYSICAL CHEMISTRY LETTERS
A JOURNAL OF THE AMERICAN CHEMICAL SOCIETY
pubs.acs.org/JPCL Letter

Nucleation and Layer Closure Behavior of Iridium Films Grown Using Atomic Layer Deposition

Hong Keun Chung, Han Kim, Jihoon Jeon, Sung-Chul Kim, Sung Ok Won, Ryosuke Harada, Tomohiro Tsugawa, Yoon Jang Chung, Seung-Hyub Baek, Tae Joo Park, and Seong Keun Kim*

Cite This: *J. Phys. Chem. Lett.* 2023, 14, 6486–6493 Read Online

ACCESS | Metrics & More | Article Recommendations | Supporting Information

ABSTRACT: Understanding the initial growth process during atomic layer deposition (ALD) is essential for various applications employing ultrathin films. This study investigated the initial growth of ALD Ir films using tricarbonyl-(1,2,3-η)-1,2,3-tri(*tert*-butyl)-cyclopropenyl-iridium and O_2. Isolated Ir nanoparticles were formed on the oxide surfaces during the initial growth stage, and their density and size were significantly influenced by the growth temperature and substrate surface, which strongly affected the precursor adsorption and surface diffusion of the adatoms. Higher-density and smaller nanoparticles were formed at high temperatures and on the Al_2O_3 surface, forming a continuous Ir film with a smaller thickness, resulting in a very smooth surface. These findings suggest that the initial growth behavior of the Ir films affects their surface roughness and continuity and that a comprehensive understanding of this behavior is necessary for the formation of continuous ultrathin metal films.

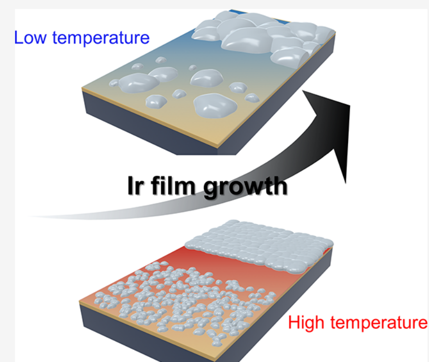

Platinum-group metals, such as Ru, Pt, and Ir, have received significant attention for various applications in microelectronics. Among them, Ir has a high oxidation resistance and a high work function (5.3 eV),[1] compared to that of Ru (4.7 eV), which is advantageous for the suppression of leakage currents of capacitors when used as electrodes in dynamic random-access memory (DRAM) capacitors.[2−6] Additionally, Ir has been considered an alternative conducting material in low-level interconnects such as metal 0 and metal 1, vias, and liners.[7] Although Cu is currently used as the conducting material for the interconnects of integrated circuits, the long electron mean free path (39.9 nm)[8] of Cu drastically increases the resistivity of the Cu layers in state-of-the-art interconnect lines (<10 nm wide). In contrast, Ir has a very short electron mean free path (7.09 nm),[8] a low bulk resistivity (4.7 $\mu\Omega$ cm), and consequently a lower resistivity at the extremely small dimensions of the next-generation semiconductor devices.

As semiconductor devices continue to shrink, the film thickness required for electrodes and interconnects in these applications decreases dramatically, which requires a novel deposition technology capable of controlling film continuity and smoothness at extremely small (<5 nm) thicknesses. Atomic layer deposition (ALD), which is based on the self-limiting mechanism of the chemical reaction between the precursor and the substrate surface,[9,10] is an effective technique for forming ultrathin films because it permits precise thickness control at the atomic scale. However, ALD of continuous ultrathin noble metal films on dielectrics is challenging. Generally, continuous ultrathin film formation using ALD requires either layer-by-layer growth from the initial stage of growth or rapid layer closure with a high density of nuclei. However, ALD of most noble metals, including Ir, does not typically exhibit this behavior,[11,12] which is mainly due to two factors, namely, the poor adsorption of metal precursors on dielectric surfaces and the large surface energy differences between noble metals and dielectrics. Poor adsorption of precursors in dielectrics suppresses the nucleation of noble metals during the initial growth stage, resulting in long incubation cycles.[11,13,14] The large difference in the surface energies induces aggregation through energy minimization, which is facilitated by the surface diffusion of adatoms,[15] resulting in nanoparticle formation at the beginning of growth. Furthermore, Grillo et al. reported that during the Pt ALD process, the Pt nanoparticles develop mainly via nanoparticle diffusion rather than via single-atom processes, including precursor chemisorption, atom attachment, and Oswald ripening.[16] Mackus et al. also reported that Pt nanoparticles grow not only by the ALD chemical reactions but also by Oswald ripening via volatilization into PtO_2.[17] Therefore, for nanoparticles to coalesce and eventually achieve layer closure, a larger thickness is generally necessary for ALD of noble metals.

Received: May 19, 2023
Accepted: July 11, 2023
Published: July 13, 2023

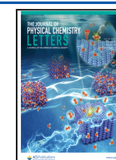

Downloaded via HANYANG UNIV on May 21, 2024 at 00:39:53 (UTC).
See https://pubs.acs.org/sharingguidelines for options on how to legitimately share published articles.

ACS Publications © 2023 American Chemical Society

https://doi.org/10.1021/acs.jpclett.3c01369
J. Phys. Chem. Lett. 2023, 14, 6486−6493

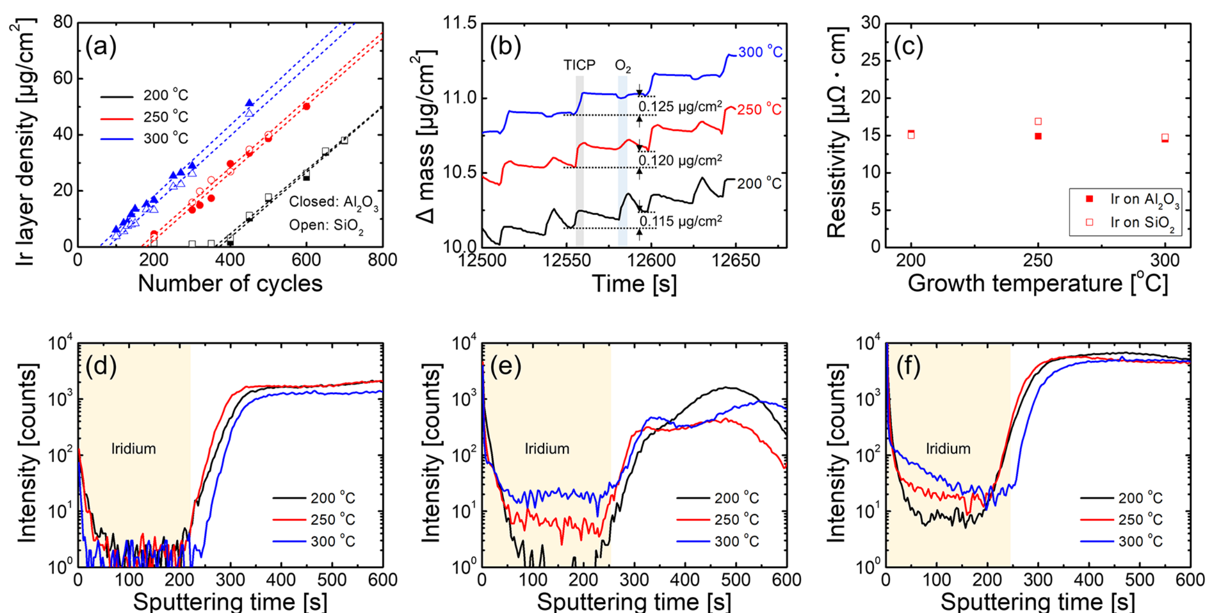

Figure 1. Growth characteristics of the ALD-grown Ir film. (a) Variation in the Ir layer density of the films grown at 200, 250, and 300 °C as a function of the number of ALD cycles. (b) QCM measurements for the Ir film grown using ALD at 200, 250, and 300 °C. (c) Variation in the bulk resistivity of Ir films grown on SiO_2 and Al_2O_3 as a function of growth temperature. SIMS depth profiles of (d) O, (e) C, and (f) H in the Ir films grown at various temperatures.

Accordingly, the formation of continuous ultrathin Ir films necessitates a comprehensive understanding of the initial growth behavior during Ir ALD. However, most studies on Ir ALD have mainly focused on ALD chemistry with various precursors and the steady-state growth behavior of Ir ALD.[18−23] Although previous ALD studies have reported growth characteristics, such as the self-saturation behavior and growth per cycle (GPC), Ir film properties, including the resistivity and impurity concentration, and step coverage over three-dimensional structured substrates,[19,24] the initial ALD growth of Ir films remains insufficiently understood. Along with the formation of continuous ultrathin Ir films, the initial growth also affects the surface roughness of the Ir films, as island evolution roughens the surface of the Ir films, which needs to be thoroughly understood.

In this study, the initial growth behavior, including nucleation and layer closure, during the ALD of Ir films was examined by using tricarbonyl-(1,2,3-η)-1,2,3-tri(*tert*-butyl)-cyclopropenyl-iridium (TICP) and O_2. The effects of the substrate surface and growth temperature on the initial growth behavior were examined. By controlling these effects, we could engineer the film continuity at ultrasmall thicknesses and surface roughness of the Ir films even with an increasing film thickness.

The ALD growth temperature is generally a critical parameter for determining the properties of ALD-grown films as well as their initial growth. Before the initial growth of Ir by ALD was investigated, the growth characteristics and properties of Ir films grown using ALD were examined in terms of the growth temperature. Figure 1a shows the variation in the Ir layer density of films grown at various temperatures as a function of the number of ALD cycles. The amount of Ir deposited on the films was linearly proportional to the number of ALD cycles at all temperatures after a certain number of incubation cycles. The steady-state GPC, which is calculated from the linearity, was approximately 0.12 μg cm^{-2} cycle^{-1} at all temperatures. Assuming that the ALD-grown Ir films have a theoretical density of 22.56 g/cm^3, the steady-state GPC corresponds to 0.052 nm/cycle, which is comparable to the previously reported value for ALD-grown Ir.[25] The invariance of the steady-state GPC with temperature was also verified using quartz crystal microbalance (QCM) analyses, as shown in Figure 1b. The change in the mass deposited per cycle at 200−300 °C was in a narrow range of 0.115−0.125 μg cm^{-2} cycle^{-1}.

Figure 1c shows the variation in the bulk resistivity of Ir films grown on SiO_2 and Al_2O_3 as a function of growth temperature. Bulk resistivity was calculated from the slope of the graph depicting the relationship between the inverse sheet resistance and the thickness of the Ir films (Figure S1). The film thickness was determined by dividing the Ir layer density by the theoretical density of Ir. The density of Ir films was found to be very close to its theoretical value (Figure S2). Therefore, the influences of interfacial and surface scattering on the resistivity can be excluded. The bulk resistivity of all Ir films was approximately 15 $\mu\Omega$ cm and was not significantly influenced by the growth temperature. This resistivity is comparable to that previously reported for ALD-grown Ir films.[18−20,25]

The impurity contents of the Ir films were also examined. According to the results of auger electron spectroscopy analysis (Figure S3), the amount of carbon and oxygen in the Ir films grown at all temperatures was below the detection limit of auger electron spectroscopy. Hence, a secondary ion mass spectrometry (SIMS) technique was employed to compare the contents below the detection limit of auger electron spectroscopy. Panels d−f of Figure 1 show the SIMS depth profiles of O, C, and H, respectively, in the Ir films grown at various temperatures. The oxygen content of the films at all of the growth temperatures was very low. This indicates that IrO_2 is not formed in this temperature range. Considering the large difference in the theoretical resistivity between Ir (4.7 $\mu\Omega$ cm[26]) and IrO_2 (49.1 $\mu\Omega$ cm along the [100] direction[27]), the low resistivity obtained in Figure 1c supports the absence of

https://doi.org/10.1021/acs.jpclett.3c01369
J. Phys. Chem. Lett. 2023, 14, 6486−6493

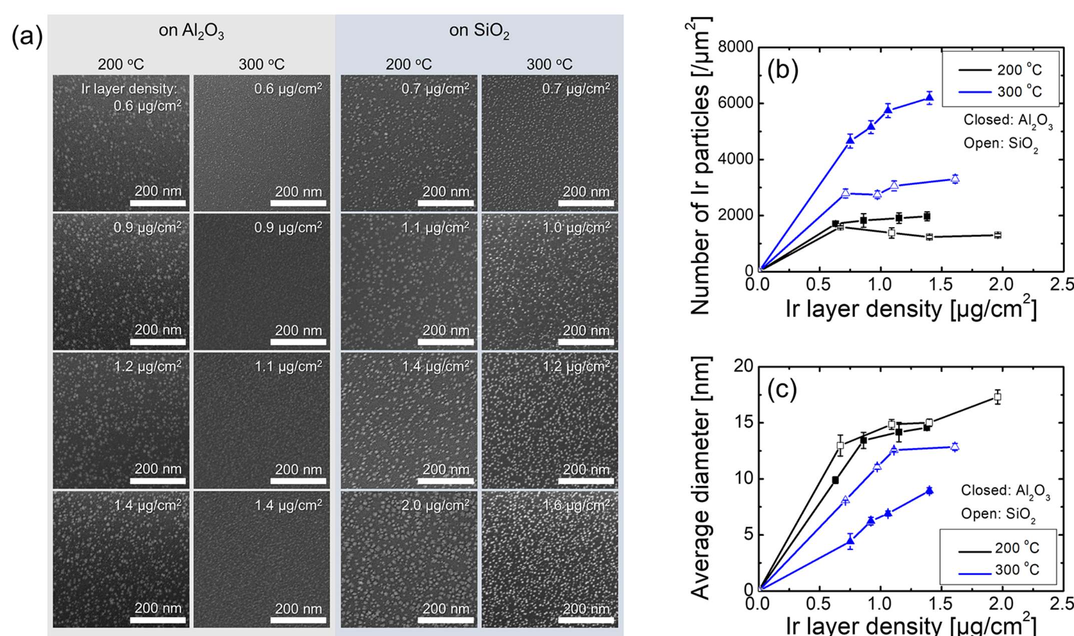

Figure 2. (a) Scanning electron microscopy images of the Ir layers deposited below 2 $\mu g/cm^2$ as a function of growth temperature (200 and 300 °C) and substrate surface (SiO_2 and Al_2O_3). Variation in the (b) density and (c) size of the Ir nanoparticles in the layers deposited below 2 $\mu g/cm^2$ as a function of Ir layer density.

IrO_2 in the films. However, the growth temperature influences the content of impurities such as C and H. The impurity content was the lowest at 200 °C, and the C and H contents increased with growth temperature. The increase in the impurity contents suggests the slight thermal decomposition of the TICP precursor above 250 °C. Although the resistivity did not vary significantly with temperature, as shown in Figure 1c, impurities should be suppressed, because they can increase the resistivity by scattering electrons and degrading thermal stability.

Although the steady-state GPC of Ir ALD was almost identical at 200−300 °C, the incubation cycle was strongly dependent on the growth temperature, as shown in Figure 1a. The number of incubation cycles for the Ir films grown at 200 °C was approximately 370. As the growth temperature increased, the number of incubation cycles decreased to 170 at 250 °C and to 77 on SiO_2 and 55 on Al_2O_3 at 300 °C. The number of incubation cycles was not significantly different for the SiO_2 and Al_2O_3 surfaces. An incubation cycle in ALD indicates the cycle period during which the adsorption of the precursor molecules is retarded during the initial growth stage. During the incubation cycle, the injected precursor molecules react with the substrate surface, creating nuclei for subsequent film growth. Therefore, the observed change in the incubation cycles as a function of the growth temperature suggests that the size and density of the Ir nanoparticles were substantially influenced by temperature.

Accordingly, the initial growth of the ALD-grown Ir film as a function of growth temperature was examined. The surface morphologies of the Ir layers deposited below 2 $\mu g/cm^2$, which corresponds to a 0.9 nm thick Ir film when converted to the nominal thickness, as a function of the growth temperature and substrate surface, are shown in Figure 2a. The figure shows that Ir nanoparticles were distributed over the substrate surface rather than forming a continuous film. The corresponding particle densities and sizes are also depicted in panels b and c, respectively, of Figure 2. The island formation suggests that the initial growth of Ir was driven by surface diffusion. It has been reported that during the initial ALD of noble metals, islands develop through the attachment of the surface-diffused adatoms.[15,16] The large difference in the surface energies between Ir [2.26 and 2.83 J/m^2 for the (111) and (100) planes,[28] respectively] and the substrate surface (0.97 and 0.26 J/m^2 for amorphous Al_2O_3[29] and SiO_2,[30] respectively) is thought to be the driver of the coalescence. Moreover, as shown in Figure 2, the nanoparticle density and size increased negligibly and significantly with the number of Ir deposition cycles. This further supports the idea that the aggregation of Ir atoms occurs via surface diffusion.

The density and size of the nanoparticles depended on the growth temperature and substrate surface. As shown in Figure 2, Al_2O_3, compared to SiO_2, had a higher particle density and a smaller particle size on its surface. This substrate surface dependence is expected because the surface energy of Al_2O_3 is larger than that of SiO_2; therefore, the driving force for aggregation is relatively smaller for Al_2O_3.

The differences in particle density and size became more pronounced with an increase in growth temperature. The particle density increased with growth temperature, whereas the particle size decreased with similar deposition amounts. Because the level of surface diffusion increases with growth temperature, particle size growth is expected at increased temperatures; however, this was not the case. It has been reported that in the initial stages of ALD of noble metals, nanoparticles mostly grow via nanoparticle diffusion and coalescence rather than through the chemisorption of single atoms and atom attachment driven by the minimization of surface energy.[16] Furthermore, nanoparticle mobility is temperature-dependent.[16] Because nanoparticle mobility increases with growth temperature, the critical size of particles at which a particle is immobilized and sticks to the substrate surface also increases.[16] The critical size at a low temperature of 200 °C is small; therefore, nanoparticles pin on the substrate. The nanoparticles act as sinks for smaller nano-

https://doi.org/10.1021/acs.jpclett.3c01369
J. Phys. Chem. Lett. 2023, 14, 6486−6493

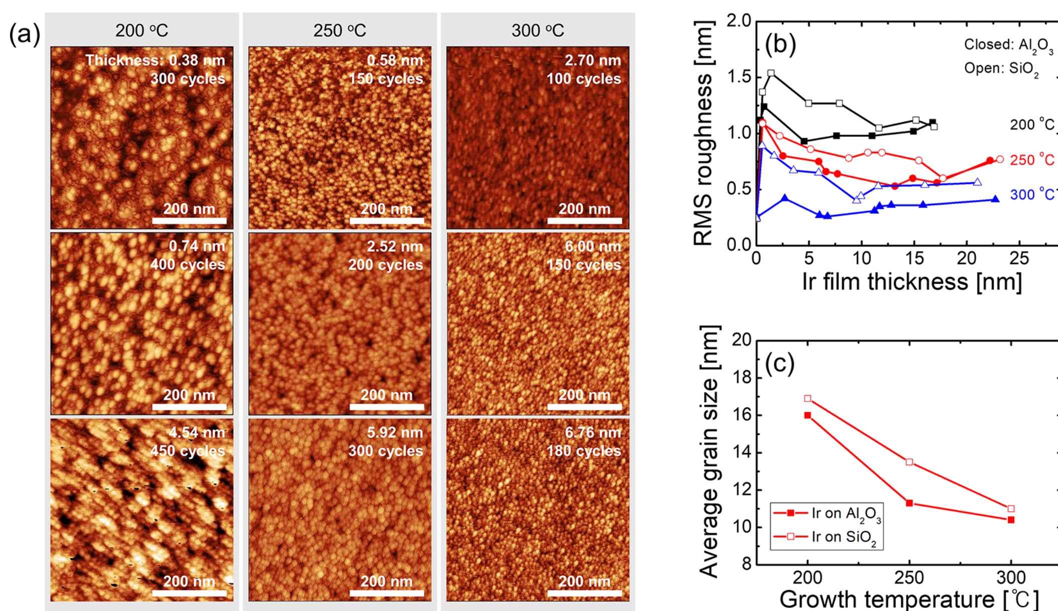

Figure 3. (a) AFM images of the surface morphologies of Ir grown on Al_2O_3 using ALD at 200, 250, and 300 °C. (b) Variation in the RMS roughness of the Ir films as a function of film thickness. (c) Variation in the average grain size of approximately 15 nm thick Ir films grown on SiO_2 and Al_2O_3 as a function of growth temperature.

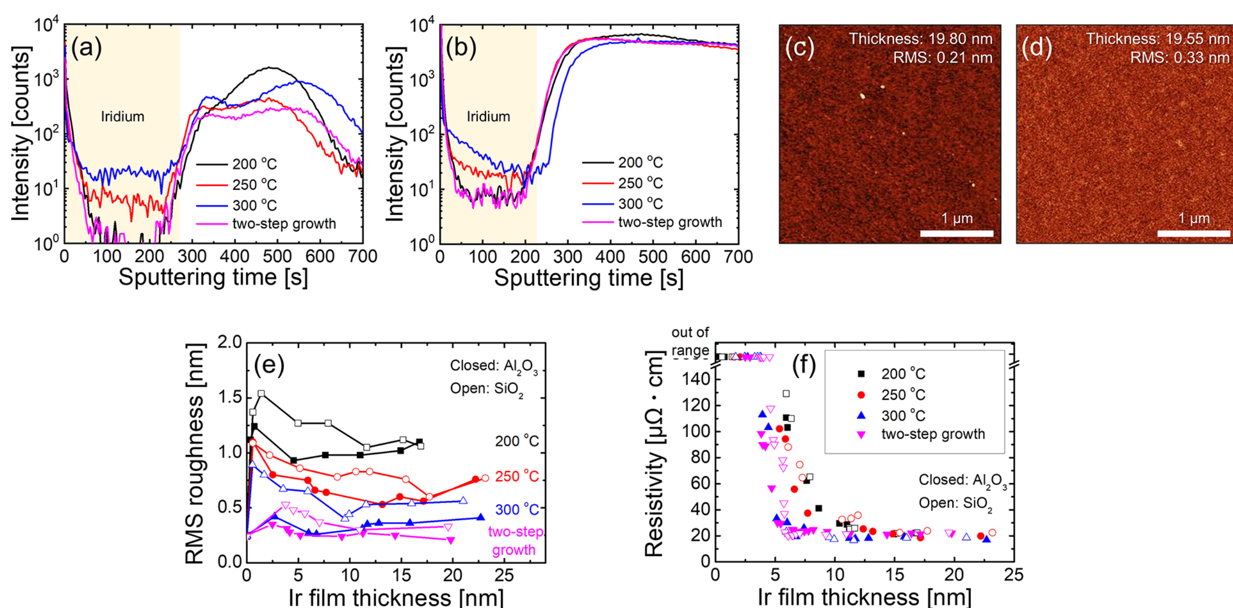

Figure 4. Various properties of two-step-grown Ir films. SIMS depth profiles of (a) C and (b) H in the two-step-grown Ir film. AFM images of the approximately 20 nm thick Ir films grown on (c) Al_2O_3 and (d) SiO_2 in two steps. (e) Variation in the RMS roughness of the Ir films, including the two-step-grown Ir film, as a function of film thickness. (f) Variation in the resistivity of the Ir films as a function of film thickness.

particles to merge around them, thereby increasing the particle size. However, the critical size at a high temperature of 300 °C is large, and the nanoparticles become mobile. Consequently, both nucleating and preexisting particles have comparable capture efficiencies, leading to the formation of small particles.

After the formation of Ir nanoparticles, a further increase in the number of ALD cycles eventually results in the formation of a thin film. However, this change in the initial growth can also affect the surface morphology of the Ir films; therefore, the surface morphologies of the ALD-grown films were observed. Figure 3a shows atomic force microscopy (AFM) images of the surface morphology of the Ir films grown on Al_2O_3 by using ALD at 200, 250, and 300 °C. Note that the thickness labeled on the AFM images corresponds to the nominal thickness calculated from the Ir layer density. Figure 3b shows the thickness-dependent variation in the root-mean-square (RMS) roughness of the Ir films in terms of the growth temperature and substrate surface, as determined using the AFM results for the Ir films up to approximately 20 nm (Figures S4–S6). The RMS roughness decreased with an increase in growth temperature and was lower on Al_2O_3 than on SiO_2. Interestingly, this characteristic of the RMS roughness variation is primarily determined during the initial growth stage prior to layer closure. Below approximately 3 nm, the RMS roughness increased considerably during the initial growth stage, where discontinuous particles are formed, and

https://doi.org/10.1021/acs.jpclett.3c01369
J. Phys. Chem. Lett. 2023, 14, 6486−6493

the value generally decreased with an increase in thickness. Consequently, the Ir film grown on SiO_2 at 200 °C with a high initial roughness had a large RMS roughness of >1 nm at a thickness of 17 nm, whereas the Ir film grown on Al_2O_3 at 300 °C with a low initial roughness had an extremely low RMS roughness of 0.4 nm at a thickness of 22.7 nm. This value was comparable to that (0.25 nm) of the Al_2O_3 substrate. It should be noted that the initial growth at 200 °C is characterized by a sparse distribution of relatively large particles, whereas the initial growth at 300 °C is characterized by a higher density of small particles. Therefore, the difference in roughness owing to variations in particle evolution at the beginning of growth influences the RMS roughness as the film thickness increases, that is, after layer closure.

The observed variation in the surface roughness of the Ir films can also be understood by the dependence of the grain size on the growth temperature and substrate surface. Figure 3c shows the variation in the average grain size of ∼15 nm thick Ir films grown on Al_2O_3 and SiO_2 as a function of growth temperature. The Scherrer equation was used to estimate the average grain size from the full width at half-maximum of the Ir (111) diffraction peak obtained using XRD analyses (Figure S7). The grain size decreased from 17 to 10 nm with an an increase in growth temperature at 200−300 °C and was slightly smaller on Al_2O_3 than on SiO_2. Facets developed on the grain surface as the grain size increased, thereby increasing the surface roughness of the Ir films. This variation in grain size was closely correlated to the density of the initially formed nanoparticles. This was valid even after continuous film formation. The formation of sparse nuclei resulted in relatively large grains, whereas the formation of dense nuclei resulted in small grains. This is consistent with the nucleation behavior shown in Figure 2 and the variation in surface roughness shown in Figure 3.

Although Ir films with smooth surfaces were formed at a high temperature of 300 °C due to dense nucleation, the content of impurities, such as C and H, increased at high temperatures. To form Ir films with a smooth surface and low impurity concentration, two-step ALD growth was attempted, in which the nucleation layer with abundant nuclei was formed at 300 °C, followed by the formation of the main layer at 200 °C. The nucleation layer was grown for 80 cycles, which is similar to the number of incubation cycles at 300 °C. Panels a and b of Figure 4 show the SIMS depth profiles of C and H, respectively, in the two-step-grown Ir film. The variation in impurities in the Ir films grown at a single temperature is also shown for comparison. The intensity of the C and H signals in the two-step-grown Ir film was extremely low and comparable to that in the Ir film grown at 200 °C. Panels c and d of Figure 4 show AFM images of approximately 20 nm thick Ir films grown on Al_2O_3 and SiO_2, respectively, in two steps. Despite their relatively large thickness of ∼20 nm, the two-step-grown Ir films were extremely smooth with an RMS roughness as low as 0.21 nm on Al_2O_3 and 0.33 nm on SiO_2. This smooth surface was attributed to the low roughness of the initial nucleation layer, which, as shown in Figure 4e and Figure S8, exhibits a slight increase in the RMS roughness with an increase in thickness.

Dense nucleation allows the formation of not only smooth surfaces but also continuous films with smaller thicknesses. Simply measuring the resistivity as the Ir thickness varies allows for the verification of continuous thin Ir films. The formation of unlinked Ir particles caused the resistivity to approach infinity. Figure 4f shows the variation in the resistivity of the Ir films as a function of film thickness. The resistivity of the two-step-grown Ir film on Al_2O_3 could be measured down to 3.8 nm. The minimum thickness for the resistivity to be measurable was comparable to the value (3.9 nm) of the Ir films grown at 300 °C and was significantly lower than the minimum thicknesses (6 nm at 200 °C and 5.4 nm at 250 °C) of the Ir films grown at 200 and 250 °C. The minimum thickness was slightly thicker on SiO_2 than on Al_2O_3. These results indicate that the two-step growth can form a continuous Ir film with a small thickness owing to the nucleation layer formed at high temperatures. Additionally, as shown in Figure 4f, the resistivity of all Ir films increased with a decrease in thickness. The thickness at which the resistivity began to increase depended on the growth temperature. The resistivity of the Ir films grown at 200 °C began to increase below approximately 10 nm, whereas the resistivity of the Ir films grown at 300 °C and the two-step-grown Ir films began to increase at 5 nm. The effect of size on resistivity is commonly observed in metal films.[31−33] The increase in resistivity is primarily attributed to electron scattering at the surfaces and grain boundaries, which are described by the Fuchs−Sondheimer[34,35] and Mayadas−Shatzkes[36,37] classical models, respectively. However, these models are not valid for explaining the size effect variation with the growth temperature for the ALD-grown Ir films. This was because the resistivity of the Ir films grown at 200 °C with larger grains began to increase with thickness. A continuous film was formed during the initial growth by connecting the preformed particles. Sparse nucleation resulted in a large height difference between the grains and the necks where the grains meet. Therefore, the increase in resistance at the necks in the Ir films grown at 200 °C resulted in a higher resistivity at the same thickness, as compared with the Ir films grown at 300 °C and two-step-grown Ir films. This was supported by the smooth surface of the Ir thin films grown at 300 °C, which had a lower resistivity at the same thickness.

A DRAM capacitor electrode is a potential application for Ir films, where the surface roughness of the electrode affects the dielectric performance, particularly the leakage current. Therefore, the leakage currents of capacitors with Ir films serving as the bottom electrodes were compared. An Ir film grown at 200 °C with a relatively rough surface and a two-step-grown Ir film with a smooth surface were used as the bottom electrodes. A 3 nm thick Al_2O_3 layer grown using ALD at 280 °C with trimethylaluminum and O_3 was used as the dielectric layer. Figure 5 shows the leakage current density versus applied voltage curves of the 3 nm thick Al_2O_3 grown on ∼6 nm thick

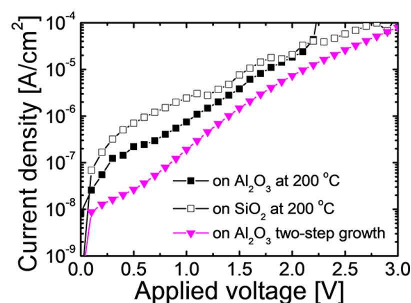

Figure 5. Leakage current density vs applied voltage curves of 3 nm thick Al_2O_3 grown on ∼6 nm thick Ir layers.

https://doi.org/10.1021/acs.jpclett.3c01369
J. Phys. Chem. Lett. 2023, 14, 6486−6493

Ir layers. Despite the same capacitance, the capacitor employing the Ir layer on SiO_2 with the highest surface roughness exhibited the highest leakage current, whereas the capacitor employing the two-step-grown Ir layer with the smallest surface roughness exhibited the lowest leakage current. The work function was verified to be the same for all Ir films (Figure S9). The capacitor employing an Ir layer on Al_2O_3 with an intermediate surface roughness exhibited moderate leakage currents. This indicates that engineering the initial growth behavior of Ir films for bottom electrodes can improve the leakage currents of the capacitors.

In summary, the initial growth behavior of Ir films grown on dielectric surfaces by using ALD and TICP and O_2 was investigated. Isolated Ir nanoparticles formed on the dielectric surfaces in the early growth stages. This is due to the preferential adsorption of the precursor on the preformed Ir surface over the dielectric surface as well as the diffusion of adatoms on the surface. The density and size of the Ir nanoparticles were significantly influenced by the growth temperature, which strongly affected the precursor adsorption and surface diffusion of adatoms. As the growth temperature increased, the density of the nanoparticles increased, whereas their size decreased. This is because despite the enhanced surface diffusion at high temperatures, the critical size at which the nanoparticles become stuck and immobile on the substrate increases with temperature. Additionally, the particles on Al_2O_3 exhibited a somewhat higher density and a slightly smaller size than those on SiO_2. This mainly resulted from a reduction in the driving force for surface diffusion on Al_2O_3. The difference in surface energy between Ir and the substrate was lower on Al_2O_3 than on SiO_2. Nanoparticle formation during initial growth also affected the properties of the Ir films even after layer closure. The formation of small and dense nanoparticles at high temperatures led to the formation of a continuous Ir film with a smaller thickness, resulting in a smooth surface. Furthermore, two-step growth, in which a nucleation layer is formed at a high temperature followed by growth at a low temperature, produced Ir films with very smooth surfaces and fewer impurities. Therefore, the insights gained from this study on the initial ALD growth of noble metals may contribute to improving the continuity and smoothness of the films required for scaled devices.

■ METHODS

Iridium thin films were grown in a custom-built chamber using ALD. The ALD process was performed in a growth temperature range of 200−300 °C. Thermally oxidized SiO_2(100 nm)/Si and ALD-grown Al_2O_3(5 nm)/SiO_2/Si coupons were used as the substrates. The substrates were exposed to an O_2 plasma at room temperature for 15 min before being loaded into the chamber. A TICP precursor (provided by TANAKA Precious Metals) and O_2 were used as the sources of Ir and O, respectively. A canister containing TICP was heated at 55 °C, and the TICP molecules were delivered into the chamber with an Ar carrier gas at 300 sccm. The flow rate of O_2 was fixed at 100 sccm. Careful control of the process parameters during ALD cycling ensured self-limiting behavior. One ALD cycle consisted of TICP feeding (8 s), purging (20 s), O_2 feeding (5 s), and purging (15 s). The number of ALD cycles was varied to vary the amount of Ir deposited.

The amount of Ir deposited on the films was estimated by using wavelength-dispersive X-ray fluorescence. The deposited amount of Ir was expressed as the layer density of Ir measured by wavelength-dispersive X-ray fluorescence. The mass change per unit area during the ALD cycles was monitored in situ using QCM. The impurity content of the films was analyzed by using time-of-flight SIMS (TOF.SIMS 5, ION-TOF GmbH). The depth profile was obtained through a dual-beam mode using a 1 keV Cs^+ etching ion beam with a current of 5 nA and a 30 keV Bi^+ analysis ion beam with a current of 1 pA. The sheet resistances of the films were measured using the four-point probe method. Resistivity was calculated by using the obtained sheet resistance and film thickness. The surface morphologies of the films were examined by using AFM and scanning electron microscopy.

■ ASSOCIATED CONTENT

Supporting Information

The Supporting Information is available free of charge at https://pubs.acs.org/doi/10.1021/acs.jpclett.3c01369.

Sheet resistance, X-ray reflectivity, auger electron spectroscopy, AFM images, XRD data, and ultraviolet photoelectron spectroscopy of the Ir films (PDF)

Transparent Peer Review report available (PDF)

■ AUTHOR INFORMATION

Corresponding Author

Seong Keun Kim − *Electronic Materials Research Center, Korea Institute of Science and Technology, Seoul 02792, South Korea; KU-KIST Graduate School of Converging Science and Technology, Korea University, Seoul 02841, South Korea;* orcid.org/0000-0001-8712-7167; Email: s.k.kim@kist.re.kr

Authors

Hong Keun Chung − *Electronic Materials Research Center, Korea Institute of Science and Technology, Seoul 02792, South Korea; Department of Materials Science and Chemical Engineering, Hanyang University, Ansan 15588, South Korea*

Han Kim − *Electronic Materials Research Center, Korea Institute of Science and Technology, Seoul 02792, South Korea; KU-KIST Graduate School of Converging Science and Technology, Korea University, Seoul 02841, South Korea*

Jihoon Jeon − *Electronic Materials Research Center, Korea Institute of Science and Technology, Seoul 02792, South Korea; KU-KIST Graduate School of Converging Science and Technology, Korea University, Seoul 02841, South Korea*

Sung-Chul Kim − *Advanced Analysis Center, Korea Institute of Science and Technology, Seoul 02792, South Korea*

Sung Ok Won − *Advanced Analysis Center, Korea Institute of Science and Technology, Seoul 02792, South Korea*

Ryosuke Harada − *Chemical Materials Development Division, TANAKA Precious Metals, Tsukuba 300-4247, Japan*

Tomohiro Tsugawa − *Chemical Materials Development Division, TANAKA Precious Metals, Tsukuba 300-4247, Japan*

Yoon Jang Chung − *Department of Chemical and Biological Engineering, Korea University, Seoul 02841, South Korea*

Seung-Hyub Baek − *Electronic Materials Research Center, Korea Institute of Science and Technology, Seoul 02792, South Korea*

Tae Joo Park − *Department of Materials Science and Chemical Engineering, Hanyang University, Ansan 15588, South Korea;* orcid.org/0000-0003-4641-2425

https://doi.org/10.1021/acs.jpclett.3c01369
J. Phys. Chem. Lett. 2023, 14, 6486−6493

Complete contact information is available at:
https://pubs.acs.org/10.1021/acs.jpclett.3c01369

Notes

The authors declare no competing financial interest.

■ ACKNOWLEDGMENTS

This research was supported by the National R&D Program through the National Research Foundation of Korea (NRF), funded by the Ministry of Science and ICT (2021M3D1A2045626), the R&D Convergence Program (CAP22031-300) of the National Research Council of Science and Technology of Korea, the MOTIE (Ministry of Trade, Industry & Energy) (1415187483) and KSRC (Korea Semiconductor Research Consortium) (23002-15FC) support program for the development of the future semiconductor device, and the KU-KIST Graduate School of Converging Science and Technology Program.

■ REFERENCES

(1) Huang, C.; Cheng, C.-H.; Lee, K.-T.; Liou, B.-H. High-performance metal-insulator-metal capacitor using quality properties of high- κ TiPrO dielectric. *J. Electrochem. Soc.* **2009**, *156*, G23.

(2) Kim, S. K.; Han, S.; Han, J. H.; Lee, W.; Hwang, C. S. Atomic layer deposition of TiO_2 and Al-doped TiO_2 films on ir substrates for ultralow leakage currents. *Phys. Status Solidi-RRL* **2011**, *5*, 262−264.

(3) Kim, S. K.; Han, S.; Jeon, W.; Yoon, J. H.; Han, J. H.; Lee, W.; Hwang, C. S. Impact of bimetal electrodes on dielectric properties of TiO_2 and Al-doped TiO_2 films. *ACS Appl. Mater. Interfaces* **2012**, *4*, 4726−4730.

(4) Cha, S. Y.; Jang, B.-T.; Kwak, D.-H.; Shin, C. H.; Lee, H. C. Iridium thin film as a bottom electrode for high dielectric $(Ba,Sr)TiO_3$ capacitors. *Integr. Ferroelectr.* **1997**, *17*, 187−195.

(5) Grill, A.; Brady, M. J. Platinum alloys and iridium bottom electrodes for perovskite based capacitors in dram applications. *Integr. Ferroelectr.* **1995**, *8*, 299−308.

(6) Cha, S. Y.; Jang, B.-T.; Lee, H. C. Effects of Ir electrodes on the dielectric constants of $Ba_{0.5}Sr_{0.5}TiO_3$ films. *Jpn. J. Appl. Phys.* **1999**, *38*, L49.

(7) Lanzillo, N. A.; Edelstein, D. C. Reliability and resistance projections for rhodium and iridium interconnects from first-principles. *J. Vac. Sci. Technol. B* **2022**, *40*, No. 052801.

(8) Gall, D. Electron mean free path in elemental metals. *J. Appl. Phys.* **2016**, *119*, No. 085101.

(9) Puurunen, R. L. Surface chemistry of atomic layer deposition: A case study for the trimethylaluminum/water process. *J. Appl. Phys.* **2005**, *97*, No. 121301.

(10) George, S. M. Atomic layer deposition: An overview. *Chem. Rev.* **2010**, *110*, 111−131.

(11) Kim, S. K.; Han, J. H.; Kim, G. H.; Hwang, C. S. Investigation on the growth initiation of Ru thin films by atomic layer deposition. *Chem. Mater.* **2010**, *22*, 2850−2856.

(12) Pyeon, J. J.; Cho, C. J.; Baek, S.-H.; Kang, C.-Y.; Kim, J.-S.; Jeong, D. S.; Kim, S. K. Control of the initial growth in atomic layer deposition of Pt films by surface pretreatment. *Nanotechnology* **2015**, *26*, No. 304003.

(13) Zhang, C.; Tois, E.; Leskelä, M.; Ritala, M. Substrate-dependent area-selective atomic layer deposition of noble metals from metal β-diketonate precursors. *Chem. Mater.* **2022**, *34*, 8379−8388.

(14) de Paula, C.; Richey, N. E.; Zeng, L.; Bent, S. F. Mechanistic study of nucleation enhancement in atomic layer deposition by pretreatment with small organometallic molecules. *Chem. Mater.* **2020**, *32*, 315−325.

(15) Soethoudt, J.; Grillo, F.; Marques, E. A.; van Ommen, J. R.; Tomczak, Y.; Nyns, L.; Van Elshocht, S.; Delabie, A. Diffusion-mediated growth and size-dependent nanoparticle reactivity during ruthenium atomic layer deposition on dielectric substrates. *Adv. Mater. Interface* **2018**, *5*, No. 1800870.

(16) Grillo, F.; Van Bui, H.; Moulijn, J. A.; Kreutzer, M. T.; van Ommen, J. R. Understanding and controlling the aggregative growth of platinum nanoparticles in atomic layer deposition: An avenue to size selection. *J. Phys. Chem. Lett.* **2017**, *8*, 975−983.

(17) Mackus, A. J. M.; Verheijen, M. A.; Leick, N.; Bol, A. A.; Kessels, W. M. M. Influence of oxygen exposure on the nucleation of platinum atomic layer deposition: Consequences for film growth, nanopatterning, and nanoparticle synthesis. *Chem. Mater.* **2013**, *25*, 1905−1911.

(18) Aaltonen, T.; Ritala, M.; Sammelselg, V.; Leskelä, M. Atomic layer deposition of iridium thin films. *J. Electrochem. Soc.* **2004**, *151*, G489.

(19) Hämäläinen, J.; Puukilainen, E.; Kemell, M.; Costelle, L.; Ritala, M.; Leskelä, M. Atomic layer deposition of iridium thin films by consecutive oxidation and reduction steps. *Chem. Mater.* **2009**, *21*, 4868−4872.

(20) Mattinen, M.; Hämäläinen, J.; Vehkamäki, M.; Heikkilä, M. J.; Mizohata, K.; Jalkanen, P.; Räisänen, J.; Ritala, M.; Leskelä, M. Atomic layer deposition of iridium thin films using sequential oxygen and hydrogen pulses. *J. Phys. Chem. C* **2016**, *120*, 15235−15243.

(21) Kim, S.-W.; Kwon, S.-H.; Kwak, D.-K.; Kang, S.-W. Phase control of iridium and iridium oxide thin films in atomic layer deposition. *J. Appl. Phys.* **2008**, *103*, 023517.

(22) Hämäläinen, J.; Hatanpää, T.; Puukilainen, E.; Costelle, L.; Pilvi, T.; Ritala, M.; Leskelä, M. (MeCp)Ir(CHD) and molecular oxygen as precursors in atomic layer deposition of iridium. *J. Mater. Chem.* **2010**, *20*, 7669−7675.

(23) Hämäläinen, J.; Hatanpää, T.; Puukilainen, E.; Sajavaara, T.; Ritala, M.; Leskelä, M. Iridium metal and iridium oxide thin films grown by atomic layer deposition at low temperatures. *J. Mater. Chem.* **2011**, *21*, 16488−16493.

(24) Mattinen, M.; Hämäläinen, J.; Gao, F.; Jalkanen, P.; Mizohata, K.; Räisänen, J.; Puurunen, R. L.; Ritala, M.; Leskelä, M. Nucleation and conformality of iridium and iridium oxide thin films grown by atomic layer deposition. *Langmuir* **2016**, *32*, 10559−10569.

(25) Park, N.-Y.; Kim, M.; Kim, Y.-H.; Ramesh, R.; Nandi, D. K.; Tsugawa, T.; Shigetomi, T.; Suzuki, K.; Harada, R.; Kim, M.; et al. Atomic layer deposition of iridium using a tricarbonyl cyclopropenyl precursor and oxygen. *Chem. Mater.* **2022**, *34*, 1533−1543.

(26) Haynes, W. M. *CRC handbook of chemistry and physics*, 95th ed.; CRC Press: Hoboken, NJ, 2014.

(27) Ryden, W. D.; Lawson, A. W.; Sartain, C. C. Electrical transport properties of IrO_2 and RuO_2. *Phys. Rev. B* **1970**, *1*, 1494−1500.

(28) Klyukin, K.; Zagalskaya, A.; Alexandrov, V. Ab initio thermodynamics of iridium surface oxidation and oxygen evolution reaction. *J. Phys. Chem. C* **2018**, *122*, 29350−29358.

(29) Tavakoli, A. H.; Maram, P. S.; Widgeon, S. J.; Rufner, J.; van Benthem, K.; Ushakov, S.; Sen, S.; Navrotsky, A. Amorphous alumina nanoparticles: Structure, surface energy, and thermodynamic phase stability. *J. Phys. Chem. C* **2013**, *117*, 17123−17130.

(30) Brunauer, S.; Kantro, D. L.; Weise, C. H. The surface energies of amorphous silica and hydrous amorphous silica. *Can. J. Chem.* **1956**, *34*, 1483−1496.

(31) Hu, C.; Zhang, Y.; Chen, Z.; Zhang, Q.; Zhu, J.; Hu, S.; Ke, Y. Size effect of resistivity due to surface roughness scattering in alternative interconnect metals: Cu, Co, Ru, and Mo. *Phys. Rev. B* **2023**, *107*, 195422.

(32) Wang, P. P.; Wang, X. J.; Du, J. L.; Ren, F.; Zhang, Y.; Zhang, X.; Fu, E. G. The temperature and size effect on the electrical resistivity of Cu/V multilayer films. *Acta Mater.* **2017**, *126*, 294−301.

(33) Ko, E. C.; Kim, J. Y.; Rhee, H.; Kim, K. M.; Han, J. H. Low-resistivity ruthenium metal thin films grown via atomic layer deposition using dicarbonyl-bis(5-methyl-2,4-hexanediketonato)-ruthenium(ii) and oxygen. *Mater. Sci. Semicon. Proc.* **2023**, *156*, 107258.

(34) Fuchs, K. The conductivity of thin metallic films according to the electron theory of metals. *Math. Proc. Camb. Philos. Soc.* **1938**, *34*, 100−108.

(35) Sondheimer, E. H. The mean free path of electrons in metals. *Adv. Phys.* **1952**, *1*, 1−42.

(36) Mayadas, A. F.; Shatzkes, M. Electrical-resistivity model for polycrystalline films: The case of arbitrary reflection at external surfaces. *Phys. Rev. B* **1970**, *1*, 1382−1389.

(37) Mayadas, A. F.; Shatzkes, M.; Janak, J. F. Electrical resistivity model for polycrystalline films: The case of specular reflection at external surfaces. *Appl. Phys. Lett.* **1969**, *14*, 345−347.

https://doi.org/10.1021/acs.jpclett.3c01369
J. Phys. Chem. Lett. 2023, 14, 6486−6493